Indian Journal of Chemistry
Vol. 60A, November 2021, pp. 1443-1451

P123 assisted sol-gel combustion synthesis of mesoporous strontium titanate nanomaterials for photocatalytic degradation of methylene blue

Juliya Acha Parambil[a,b], Abdul Mujeeb V M[b] & Sreenivasan Koliyat Parayil[a,*]

[a]University of Calicut Approved Research Centre in Chemistry, MES Kalladi College, Mannarkkad, Kerala 678 583, India

[b] Department of Chemistry, University of Calicut, Malappuram, Kerala 673 635, India

*E-mail: drsreenivasan@meskc.ac.in

Received 30 July 2021; revised and accepted 26 October 2021

We have reported the synthesis of strontium titanate (ST) nanomaterials via sol-gel combustion method in the presence and absence of pluronic P123 as a templating agent and citric acid as fuel at relatively high temperature. The presence of templating agent and fuel helps to generate mesoporosity in the materials resulting in mesoporous strontium titanate (MST). The materials are well characterized by various instrumental techniques. X-ray powder diffraction analysis has confirmed that both of the strontium titanate materials exhibited cubic perovskite structure. The FT-IR spectra has indicated that during high temperature calcination, carbonate species expelled out from the decomposition of the volatile impurities get adsorbed on the surface of titanate nanostructure, which is predominant in MST as indicated by the variation in the intensity of peak in between 1450 cm^{-1} –1470 cm^{-1}. From diffuse reflectance spectra, the absorption edge of the MST is extended to visible regions and showed band gap energy of 3.14 eV compared to 3.21 eV for ST. The reduction in intensities of PL emission bands in MST compared to ST has indicated that slow electron-hole recombination takes place in this material compared to ST. The Transmission electron microscopic studies reveal the formation of spherical and cuboidal nanostructures with an average size of 55 and 38 nm for ST and MST material, respectively. From N_2 sorption studies, the MST exhibit type IV adsorption isotherms with H3 type hysteresis loop indicated the formation of mesoporosity in this material whereas the ST indicated the formation of type II adsorption isotherms typical of nonporous materials. The elemental analysis of MST material is further confirmed from X-ray photoelectron spectroscopic analysis and confirm the formation of carbonate species on the surface of the materials. The photocatalytic activity of the materials is elucidated by the degradation of methylene blue under UV light irradiation and degradation followed first order kinetics with Langmuir-Hinshelwood adsorption pathways. The activity of MST material is found to be 5 times faster than ST at similar experimental conditions. The enhanced activity of the MST might be attributed to, lower band gap energy, presence of carbonate species, and lower electron-hole recombination in this material.

Keywords: Sol-gel combustion synthesis, Pluronic P123, Citric acid fuel, High temperature calcination, Mesoporous strontium titanate, Photocatalysis, Dye degradation

The rapid advancement in the industrial sector has become a major factor for ecological imbalance and effective methods are to be identified to alleviate environmental issues. Complete mineralization of hazardous pollutants using photocatalysis is a proficient method to scale down the environmental impacts of industrialization[1]. The photocatalytic performance of a catalyst is dependent upon the effectiveness of charge separation and absorption of light. The strontium titanate (ST) ($SrTiO_3$) can be considered as an effective photocatalyst for various purposes like degradation of pollutants, dyes, antibiotics, water splitting, and CO_2 reduction[2]. The superior characteristics of strontium titanate, like stability in chemical and structural aspects, resistance to heat, and corrosion have triggered the application of this material in the field of photocatalysis[3]. Liang *et al.* synthesized ST *via* the sol-gel route for the photocatalytic degradation of nitrogen oxides (NO_x) and observed that calcination temperature and light condition have a pronounced influence on the photocatalytic activity[4]. Henrique *et al.* developed a conventional method for the synthesis of ST microsphere to undergo pH-dependent degradation of methylene blue (MB) and Rhodamine B[5]. Macaraig *et al.* conducted a comparative study on photocatalytic H_2 generation using ST nanoparticles and nanofibers and reported that the mesoporous nanofibers showed the highest photocatalytic activity[6].

The usage of textile dye has become a major issue related to industrial pollution. Synthetic dye such as

MB became a major ecological pollutant. Tarawipa *et al.* employed mesoporou sstrontium titanate (MST) nanocrystals *via* a surfactant-assisted sol-gel method for the degradation of methyl orange[7]. Kumar *et al.* synthesized phase pure samples of $BaSn_{1-x}Ni_xO_3$ with cubic crystal via solid state ceramic route[8]. There are numerous methods employed for the synthesis of MST nanomaterials[9-11]. A facile solvothermal method for the synthesis of mesoporous film of ST for photosensitized solar devices was reported by Burnside *et al*.[9]. Zheng *et al*. synthesized mesoporous Nd-doped ST nanospheres and nanoplates with high specific surface areas and excellent photocatalytic activity via microwave assisted solvothermal method[10]. Kayaalp *et al.* reported the synthesis of MST for MB degradation by using the cooperative assembly of metal chelate complexes and alkoxysilanes[11]. The sol-gel method was adopted for the synthesis of materials with purity, crystallinity and uniform particle distribution[12-14]. Therefore sol-gel combustion method has been considered as one of the cost-effective methods for the synthesis of pure, homogenous, and crystalline oxide powder[15,16]. Bhagwat *et al*. synthesized cobalt ferrite nanoparticles via the sol-gel combustion method in the presence of various fuels such as ethylene glycol, glycine, and urea and studied the influence of these fuels on the structural, morphological, and magnetic properties of cobalt ferrite[17]. From the results obtained, it was inferred that the particle size of the synthesized material was influenced by the fuel employed during sol-gel combustion.

Notably to our best of knowledge, synthesis of mesoporous strontium titanate using pluronic polymer or other carbonaceous sources is rarely reported. Existing literature lacks (i) sol-gel combustion strategy for the preparation of MST using carbonaceous sources, (ii) influence of mesoporosity of ST on the photocatalytic degradation of MB in comparison with nonmesoporous ST materials.

In our present work, we demonstrated the preparation of MST and ST by the sol-gel combustion method in the presence and absence of nonionic triblock co-polymer pluronic P123 as a structure directing agent. The materials were well characterized by various experimental techniques. The photophysical properties of the material were studied by the photodegradation of MB under UV light irradiation. The influence of pore size, crystallinity, surface area, band gap, morphology, luminescent properties, and elemental composition on the surface of the materials was well studied. The photodegradation ability of the MST and ST were studied by using MB as a model pollutant.

Materials and Methods

Synthesis of MST and ST

Titanium (IV) isopropoxide (TTIP; AR grade 97%), ethylene glycol (EG; AR grade 99%), citric acid (AR grade 99%), strontium nitrate $Sr(NO_3)_2$ (AR grade 99%), pluronic P123 (AR grade), and ethanol (AR grade 99 %) were purchased from Sigma Aldrich. For the synthesis of MST, about 0.2 g of pluronic P123 was dissolved in 60 mL ethanol and stirred for 2 h. 6.5 mL titanium isopropoxide solution was added to the above reaction mixture followed by the addition of 6.7 mL ethylene glycol, and 6.6 mL water. The resulting solution was stirred continuously for 2 h. About 35 mL 6.3 g citric acid was added dropwise with stirring to the above solution and stirred for 10 min. This was followed by the addition of 25 mL of 4.23 g $Sr(NO_3)_2$, refluxed for 4 h at 80 °C, and kept in an oven at 100 °C for 24 h to obtain the dried gel. It was followed by calcination in a closed crucible at 800 °C for 3 h in a muffle furnace. The obtained material was labeled as mesoporous $SrTiO_3$ (MST). The same procedure was repeated in the absence of pluronic P123 to obtain ST.

Characterization techniques

The X-ray powder diffraction patterns were recorded on Bruker AXS D8 advance diffractometer using Cu-Kα radiation (λ=1.5406 Å). The FT-IR spectra of the materials were analyzed using Jasco-FTIR-4100 spectrophotometer in the range 4000-400 cm^{-1}. The Jasco-V-550-UV/VIS spectrophotometer was used to record UV-visible absorbance spectra using diffuse reflectance accessories. The photoluminescence (PL) spectra of the materials were measured by the Perkin Elmer LS55 PL spectrophotometer. The JEOL/JEM 2100 transmission electron microscope was used to obtain the HR-TEM image of the materials. BET surface areas and pore size distribution of the materials were analyzed by the BELSORP-max instrument. The elemental compositions of MST material were determined by X-ray photoelectron spectroscopic technique (XPS) using the instrument Axis Ultra, Kratos Analytical, the UK with an Al-Kα (1486.6 eV) source.

Photocatalytic degradation studies

In order to study the photocatalytic efficiencies of the MST and ST materials, photocatalytic degradation

studies were conducted on a photoreactor. About 0.2 g of catalyst was added to 50 mL MB at a concentration of 1×10^{-4} M taken in a beaker. The solution was stirred for 30 min in the UV reactor in the absence of light to maintain the adsorption-desorption equilibrium. After that the photocatalytic reaction was performed in the photoreactor of model LZC-4X- Luzchem photoreactor with UV light intensity 600 lux. The reaction was monitored by withdrawing 3 mL aliquots at an interval of 20 min. The solution was centrifuged to eliminate the effects of scattering prior to record the absorption spectra.

Results and Discussion

XRD analysis

The XRD patterns of strontium titanate obtained from the standard JCPDS file, ST and MST samples were shown in Fig. 1. The peaks at 2θ angles 22.6°, 32.3°, 39.9°, 46.4°, 57.6°, and 67.6°, can be indexed to (100), (110), (111), (200), (211), and (220) planes of ST with cubic perovskite structure[18-20]. The peak at 25.1 can be indexed to (101) plane of $SrCO_3$ formed during the heat treatment process[21]. The dislocation density was calculated by using Williamson and Smallman's formula, $\delta = 1/D^2$ where, D is particle size. The average crystallite size determined using the Debye-Scherrer equation for ST and MST was found to be 27.6 nm and 25.4 nm, respectively. Crystallite size could affect the textural properties and photogenerated electron-hole pair recombination. By increasing the surface area, more reactant species might be getting adsorbed on the surface the materials. As the crystallite size decreases the path of the charge to migrate to surface of the photocatalysts also decreases, resulting in lower recombination rate of the charge carriers. Therefore, the size of the particle can affect photocatalytic process. The dislocation densities of ST and MST were 0.13 and 0.15, respectively. The dislocation density is inversely as the crystallite size. Therefore the MST material showed higher dislocation density as compared to ST.

FT-IR analysis

FT-IR spectra obtained for ST and MST are shown in the Fig. 2. The bands at 857 and 570 cm^{-1} were ascribed to the stretching vibration of Sr-O and Ti-O bond, respectively[22]. The peak at 570 cm^{-1} was broadened for ST. The peak at 1453 cm^{-1} arises from CO_3^{2-} vibration[23]. The intensity of this peak was high in MST indicating the presence of more carbonate species on this material[24]. Increase in the peak intensity usually means an increase in the amount of the carbonate species associated with the molecular bond. The band at 1453 cm^{-1} was slightly blue shifted compared to ST. The blue shift of the peak in MST might have aroused due to the adsorption of more carbonate species on the surface of MST[25] resulting the variation in electron distribution in molecular bond.

UV-visible DRS analysis

UV-visible diffuse reflectance spectrum (DRS) was shown in Fig. 3a. The spectrum of ST shows a cut off wavelength at 319 nm whereas MST shows an absorption edge at 414 nm. The absorption spectra of MST showed a slight red shift in comparison with the spectra of ST due to the mesoporous nature of the material. The reflectance spectra was further analyzed with Kubelka-Munk theory to estimate the band gap energy (Fig. 3b). The Kubelka-Munk

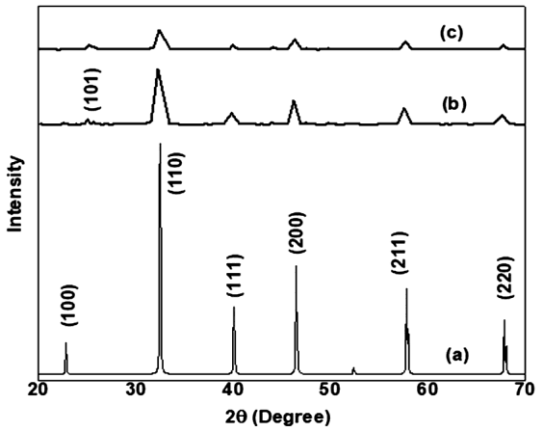

Fig. 1 — XRD patterns of (a) standard JCPDS data of strontium titanate, (b) synthesized ST and (c) MST materials

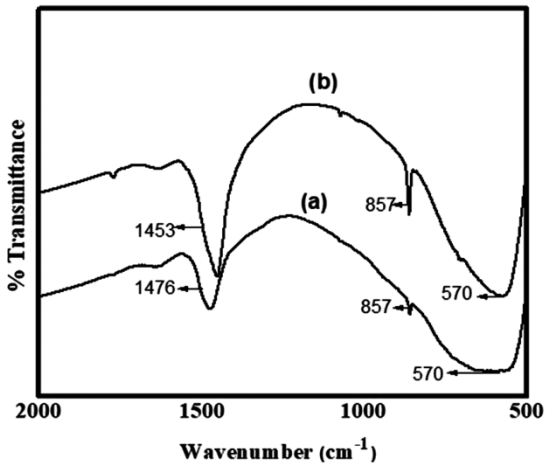

Fig. 2 — FT-IR spectra of (a) ST and (b) MST materials

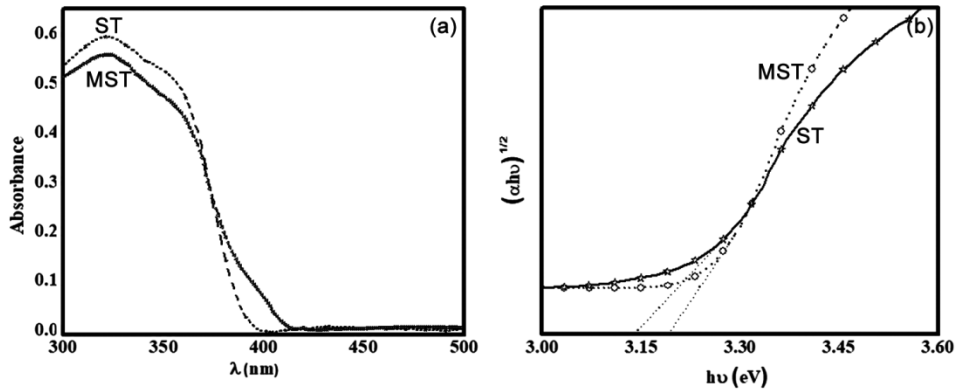

Fig. 3 — (a) UV-visible DRS spectra and (b) Kubelka-Munk plots of ST and MST materials

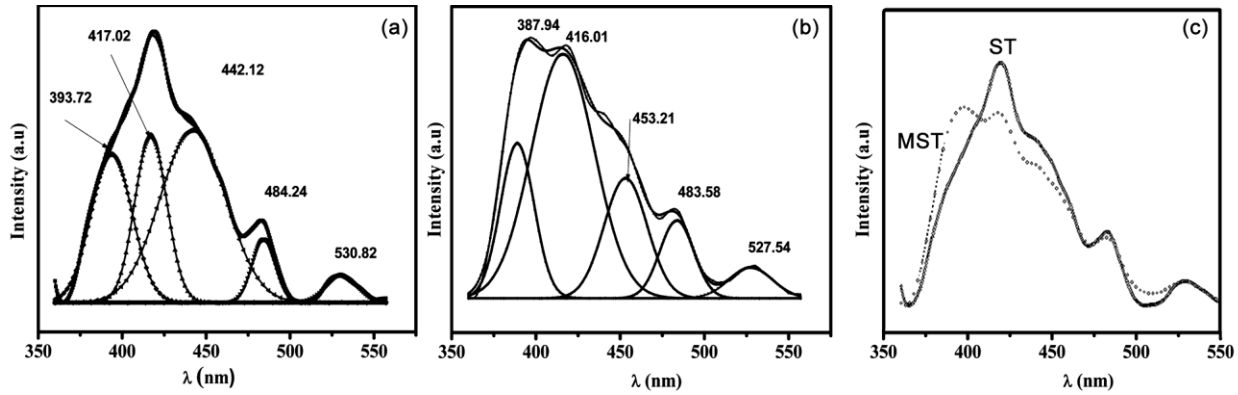

Fig. 4 — PL emission spectra originate from various defect levels of (a) ST and (b) MST and (c) for relative PL intensities

function is given by $F(R) = (1-R)^2/2R$, where, *R* is the reflectance. The bandgap energy decreased from 3.21 eV to 3.14 eV for MST compared to that of ST. Therefore in MST, the absorption edges extended to the visible regions. The reduction in the bandgap could be attributed to the attenuated light scattering by the mesoporous structure[26].

PL studies

The broad PL emissions observed for MST and ST are shown in Fig. 4a and Fig. 4b, respectively. The modification of MST has resulted in an appreciable change in the PL intensity. The resolved peaks exhibited in Fig. 4a are associated with various transitions occurred due to its high sensitivity towards visible light. The same results are also obtained for MST with slightly displaced peak centers. The emission band at 393 nm and 387 nm are related to shallow defect levels in ST[27]. The intense broad emission at 417 and 416 nm have resulted from the recombination of excited electrons and holes through the defect level and the emission at 442 and 453 can be attributed to the recombination of excited electrons and holes through their self-trapped excited states[28,29]. The other two emissions are relatively weak and are deep level defect correlated emissions[30]. The PL intensity of MST was quenched in comparison to that of ST (Fig. 4c). This might be due to the better charge separation in the mesoporous structure that resulted in the higher density of charge carriers.

BET analysis

The effect of pluronic acid on the surface area of the MST and ST was studied by N_2 adsorption-desorption isotherms. The isotherms are shown in Fig. 5. The isotherm of MST shown in Fig. 5a indicates the presence of type IV pattern with H3 type hysteresis loop. This might be due to the existence of well-developed mesopores with slit-like pores with non-uniform size and shape[31,32]. The isotherms of MST indicates typical type IV curve with monolayer adsorption at low values of relative pressures (P/P_0), followed by multilayer adsorption and capillary condensation at a relative pressure of 0.46-0.94 P/P_0. The isotherm for material ST shown in Fig. 5b indicates the presence of type II adsorption-desorption isotherm, which is typically characteristic

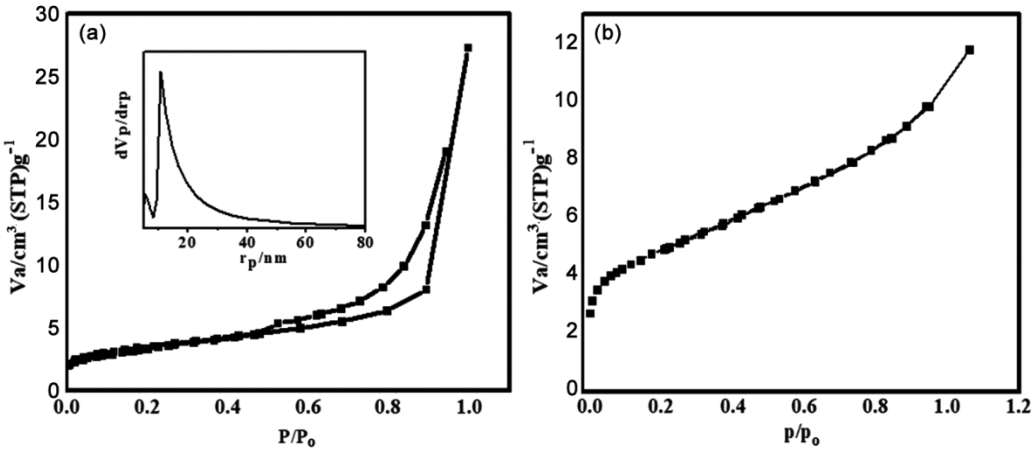

Fig. 5 — N_2-sorption isotherms of (a) MST and (b) ST along with the corresponding pore size distribution plot for MST is also shown in the inset of (a)

of nonporous materials. The specific surface area calculated from the BET adsorption isotherms of MST and ST were 12 and 17 m^2/g, respectively. The pore diameter was calculated from Barrett–Joyner–Halenda (BJH) equation, $V_n = R_n(\Delta V_n) - R_n \Delta t_n \Sigma c_i A_i$, using the desorption isotherm ,where, V_n is the volume of the pores involved in the nth desorption step, the constants R_n and c_i depend on the average pore size and average thickness of the physically adsorbed multilayer, respectively, and Δt_n is the decrease in thickness of the multilayer as a result of the nth desorption step and A_i the surface area of the set of pores involved in the ith desorption step[33]. The formation of mesopores in ST can be explained by the soft structure-directing assembly and hard-templating chemistry[34]. In presence of the structure directing agent pluronic P123, the condensation and aggregation of Sr-O-Sr occur at the polymer template/water interface[35]. The citric acid addition resulted in the effective control of the hydrolysis-condensation process of metal precursors[36]. The citrate complex promoted the interparticle interaction by stabilizing and interlinking the metal ion resulting in the organization of strontium titanate crystals around the micelles of the polymer template[37]. During calcination, the combustion of citrate complex results in the carbonization of pluronic P123 to form in situ carbon residues that act as template producing materials with mesostructures[37].

TEM studies

The HR-TEM images of ST and MST are shown in Fig. 6. The average particle size of spherical and cuboidal structures in ST and MST are found to be 55 nm and 38 nm, respectively. The results confirmed that the particles are in the nanometric regime. The measurements obtained from the SAED patterns for ST and MST samples are in consistent with the ST plane space and clearly provided a deep understanding of the perovskite structure of titanate nanostructure.

XPS studies

We investigated the elemental composition of the prepared MST material by XPS. The XPS spectrum of oxygen binding energy regions shown in Fig. 7a indicates two main peaks at 529.2 and 531.4 eV corresponding to the lattice oxygen and surface adsorbed oxygen, respectively[38]. The peaks in the XPS spectra of MST in Fig. 7b around 458.05 and 463.8 eV are attributed to Ti $2p_{3/2}$ and Ti $2p_{1/2}$, respectively[39]. The difference in the binding energy of 5.8 eV explains the valency of Ti as Ti^{4+}. The $Ti2p_{1/2}$ component located at 460.35 eV corresponds to the C-Ti-O_x bond[39]. In Fig. 7c, the peaks at binding energy values 133.05 and 134.45 eV corresponds to $Sr3d_{5/2}$ and $Sr3d_{1/2}$ in which Sr is present in Sr^{+2} oxidation state[39].The C1s peaks in Fig.7d at 279.5 eV, 284.6eV and 289.6eV corresponds to characteristics bands of C-Ti, C−C, and C=O, respectively[40,41]. The results of XPS analysis confirmed the successful synthesis of $SrTiO_3$.

Photocatalytic degradation studies

Photocatalytic degradation of MB was performed using MST catalyst whose performance was compared with that of ST catalyst. The absorption spectra of MB degradation recorded for ST and MST catalysts are depicted in the Fig. 8a and Fig. 8b, respectively. In the comparative study on

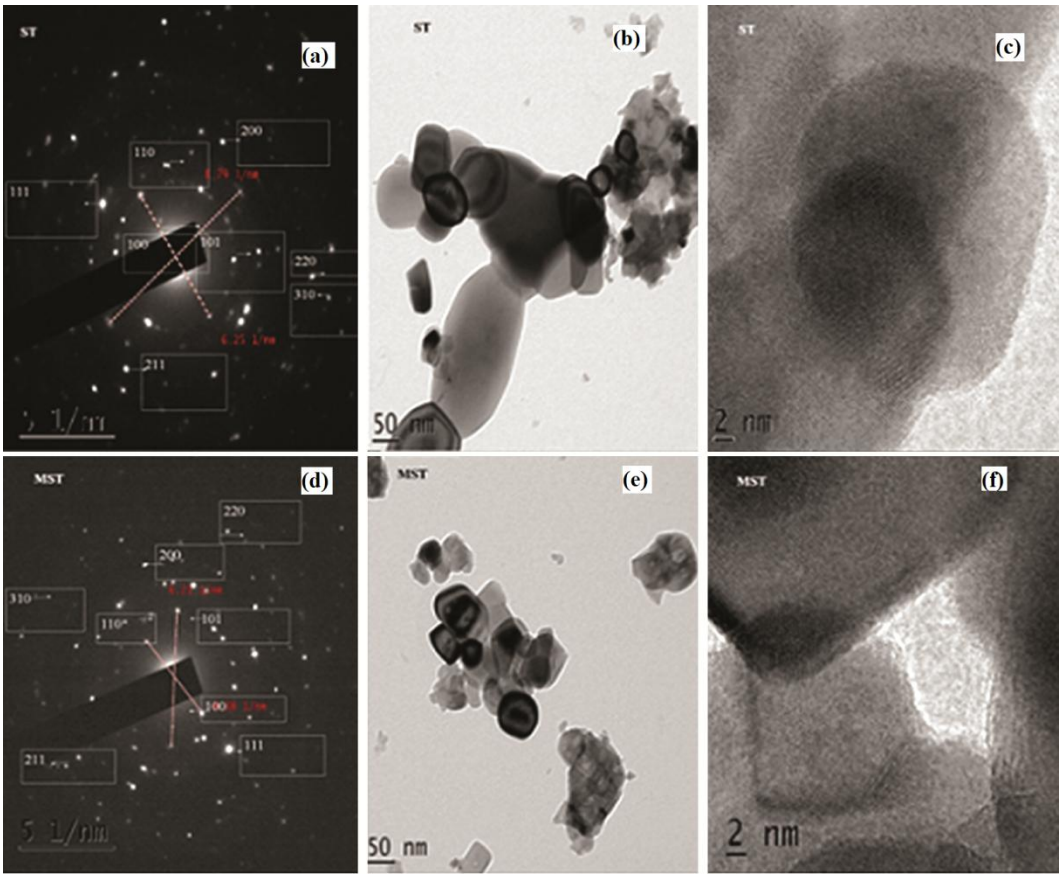

Fig. 6 — (a, d) SAED patterns, (b,e) TEM images and (c, f) HR-TEM images of ST and MST materials

photocatalytic activity using 10^{-4} M MB solution under UV source of illumination, the complete degradation of MB was achieved within a time period of 120 min. The efficiency of the degradation experiment was evaluated by using the following equation

$$\text{Degradation percentage} = [(C_0-C_t)/C_0] \times 100\%$$

where, C_0 and C_t represent the concentration of methylene blue at the time '0' and 't', respectively. Fig. 8c illustrates the degradation efficiency of MB versus irradiation time using MST and ST catalysts. It could be observed that the degradation efficiency of MB enhanced greatly in the presence of MST catalyst. Fig. 8d indicates a linear relationship between $\ln(C_0/C)$ and time, illustrating that the photocatalytic degradation of MB followed the first-order kinetics. The rate of degradation experiment can be expressed using the following equation

$$\ln(C_0/C) = kt,$$

Where, C_0 is the initial concentration of the dye methylene blue, C is the concentration of methylene blue at time t, k is the apparent rate constant.

In Fig. 8d, $\ln(C_0/C)$ varies linearly with time which indicates the first-order kinetics with regression coefficient of 0.95 and 0.85 for ST and MST, respectively. The values of the rate constant obtained for ST and MST materials were 0.007 and 0.04, respectively. The photocatalytic activity of MST is found 5.65 times faster than ST as the mesoporous structures possessed nanoscale channel walls that allowed the rapid arrival of the photogenerated electrons and holes to the surface[42]. This enhances the charge transfer efficiency and suppresses the electron-hole recombination. Moreover, the low bandgap and high density of charge carriers in MST samples facilitated the higher activity of MSTcompared to that of ST. The argument was well supported by DRS spectra and PL measurement. In the case of the ST photocatalyst, the low photocatalytic activity might be due to the formation of non-porous structures. The degradation mechanism in this structure recites as follows, on irradiation with UV light the electrons in the valence band of ST are promoted to the conduction band thereby leaving holes in the valence band. The holes react with surface adsorbed water

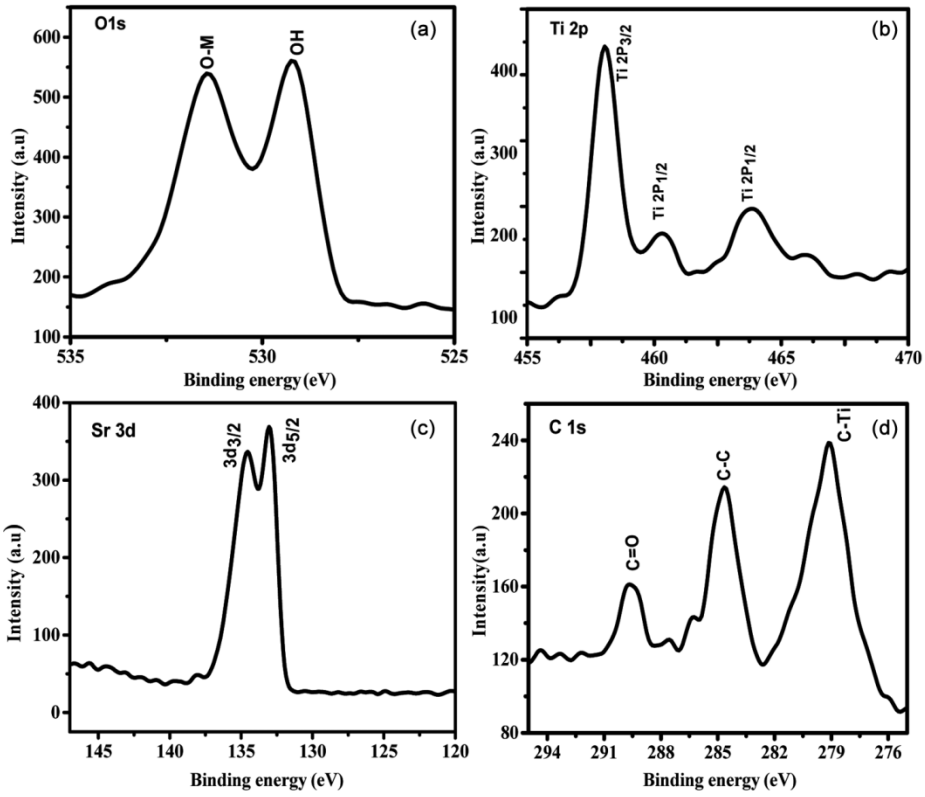

Fig. 7 — High-resolution XPS spectra of MST: (a) O 1s region, (b) Ti 2p region, (c) Sr 3d region, (d) C 1s region

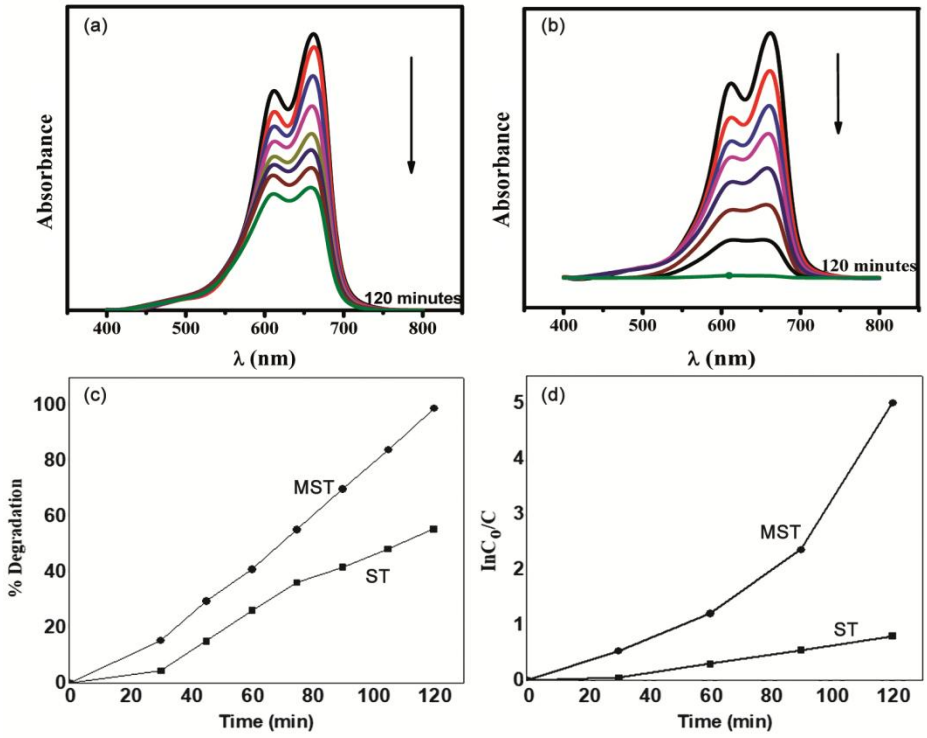

Fig. 8 — UV absorption spectra of photocatalytic degradation of MB in the presence of UV light irradiation: (a) ST as photocatalyst, (b) MST as photocatalyst, (c) percentage of degradation of MB using ST and MST photocatalyst materials and (d) $\ln(C_0/C)$ versus time of MB degradation using ST and MST photocatalyst material

producing hydroxyl radicals ($OH^{\cdot}$) whereas the electrons in the conduction band react with dissolved oxygen generating superoxide anions ($O_2^{-\cdot}$) which subsequently reacts with H^+ to generate hydroxyl radicals ($OH^{\cdot}$). The hydroxyl radicals ($OH^{\cdot}$) with high oxidizing ability degrade the MB dye. The high density of charge carriers presents in the mesoporous structures enabled the complete degradation of MB[43].

Conclusions

Mesoporous strontium titanate nanomaterial was synthesized by a cost-effective sol-gel combustion method with high chemical purity and pronounced crystallinity using pluronic P123 and citric acid as a structure-directing agent and complexating agent respectively. Citric acid addition resulted in the enhanced purity and crystallinity of the samples. The present study revealed that the triblock copolymer was essential for the generation of mesostructure.The measurements obtained from the SAED pattern for ST and MST samples are in consistent with the strontium titanate crystal plane obtained from XRD results. The UV-visible DRS spectra showed a significant reduction in band gap energy when samples were reformed into mesoporous. The photoluminescence studies showed various excitations and transitions favorable for photocatalytic activity. The study summarizes that the MST is an excellent photocatalyst that can degrade methylene blue effectively. Moreover, the photocatalytic performance of MST prepared using P123 was enhanced 5.65 times faster than ST. The high photocatalytic activity of MST compared to that of ST can be attributed to the low band gap, mesoporous structure, presence of carbonate species, and enhanced charge transfer efficiency of MST. Based on the observations we can conclude that MST synthesized using pluronic P123 is a promising photocatalytic material for the environmental remediation process and also for related applications.

Acknowledgments

The authors are grateful to department of Chemistry, University of Calicut, for proving facilities for FT-IR, UV-visible DRS measurements. The authors are grateful to CSIF, University of Calicut for BET and pore size distribution analysis. The authors would like to acknowledge the Sophisticated Test and Instrumentation Centre (STIC CUSAT) for rendering the instrumentation facilities for HR-TEM measurement. The authors acknowledge Amrita Institute of Nanoscience for X-ray photoelectron spectroscopic studies. One of the authors, Mrs. Juliya A.P is thankful to the University of Calicut for the Ph.D. studentship.

References

1 Varma K S, Tayade R J, Shah K J, Joshi P A, Shukla A D & Gandhi V G, *Water-Energy Nexus*, 3 (2020) 46.
2 Li J, Bai H, Yi W, Liu J, Li Y, Zhang Q, Yang H & Xi G, *Nano Res*, 9 (2016) 1523.
3 Zhao W, Zhao W, Zhu G, Lin T, Xu F & Huang F, *CrystEngComm*, 17 (2015) 7528.
4 Chen L, Zhang S, Wang L, Xue D & Yin S, *J Cryst Growth*, 311 (2009) 746.
5 Mourão H A J L, Lopes O F, Ribeiro C & Mastelaro V R, *Mater Sci Semicond Process*, 30 (2015) 651.
6 Macaraig L, Chuangchot S & Sagawa T, *J Mater Res*, 29 (2014) 123.
7 Puangpetch T, Sreethawong T, Yoshikawa S & Chavadej S, *J Mol Catal A Chem*, 287 (2008) 70.
8 Kumar U, Ansaree M J, Verma A K, Upadhyay S & Gupta G, *Mater Res Express*, 4 (2017) 116304.
9 Burnside S, Moser J E, Brooks K, Gratzel M & Cahen D, *J Phys Chem B*, 103 (1999) 9328.
10 Zheng J Q, Zhu J Y, Xu J S, Lu B Q, Qi C, Chen F & Wu J, *Mater Lett*, 100 (2013) 62.
11 Kayaalp B E, Lee Y J, Kornowski A, Gross S, D'Arienzo M & Mascotto S, *RSC Adv*, 6 (2016) 9040.
12 Kumar A, Khan B, Singh G, Dixit A, Kumar U, Singh M K, *Phys Scr*, 95 (2020) 105807.
13 Cheema H, Yadav V, Maurya R S, Yadav V, Kumar A, Sharma N, Alvi P A & Kuma U, *J Mater Sci: Mater Electron*, 32 (2021) 23578.
14 Vinogradov A V & Vinogradov V V, *RSC Adv*, 4 (2014) 45903.
15 Shi L, Zeng C, Jin Y, Wang T & Tsubaki N, *Catal Sci Technol*, 2 (2012) 2569.
16 Xia G, Zhou S, Zhang J & Xu J, *J Cryst Growth*, 279 (2005) 357.
17 Bhagwata V R, Humbe A V, More S D& Jadhav K M, *Mater Sci Eng B*, 248 (2019) 114388.
18 Kangaraj T & Thiripuranthagan S, *Appl Catal B*, 207 (2017) 218.
19 Xia Y, He Z, Lu Y, Tang B, Sun S, Su J & Li X, *RSC Adv*, 8 (2018) 5441.
20 Ha M N, Zhu F, Liu Z, Wang L, Liu L, Lu G & Zhao Z, *RSC Adv*, 6 (2016) 21111.
21 Li L, Lin R, Tong Z & Feng Q, *Nanoscale Res Lett*, 7 (2012) 305.
22 Wu Z, Zhang Y, Wang X & Zou Z, *New J Chem*, 41 (2017) 5678.
23 Lu P, Hu X, Li Y, Zhang M, Liu X, He Y, Dong F, Fu M & Zhang Z, *RSC Adv*, 8 (2018) 6315.
24 Dahm S & Risnes S, *Calcif Tissue Int*, 65 (1999) 459.
25 Shahabuddin S, Sarih N M, Mohamad S & Ching J J, *Polymers*, 8 (2016) 27.

26 Zou F, Jiang Z, Qin X, Zhao Y, Jiang L, Zhi J, Xiao T & Edwards P P, *Chem Comm*, 48 (2012) 8514.

27 Tamiolakis I, Liu D, Xiao F X, Xie J, Papadas I T, Salim T, Liu B, Zhang Q, Choulis S A & Armatas G S, *Appl Catal B*, 236 (2018) 338.

28 Singh S, Lakshminarayana G, Sharma M, Dao T D, Chen K, Wada Y, Takeda T & Nagao T, *J Spectrosc*, 2015 (2015) 493607.

29 Samokhvalov A, *Phys Chem Chem Phys*, 23 (2021) 7022.

30 Kumar V, Choudhary S, Malik V, Nagarajan R, Kandasami A & Subramanian A, *Phys Status Solidi A*, 216 (2019) 1900294.

31 Wang Z, Jiang X, Pan M & Shi Y, *Minerals*, 10 (2020) 377.

32 Leofanti G, Padovan M, Tozzola G & Venturelli B, *Catalysis Today*, 41 (1998) 207.

33 Masthan S K, Rao K S R, Prasad P S S & Rao P K, *Adsorp Sci Technol*, 4 (1992) 212.

34 Lee J, Orilall MC, Warren S C, Kamperman M, DiSalvo F J & Wiesner U, *Nat Mater*, 7 (2008) 222.

35 Subha N, Mahalakshmi M, Myilsamy M, Reddy N L, Shankar M V, Neppolian B & Murugesan V, *Colloids Surf A*, 522 (2017) 193.

36 Liu G, Liu Y, Yang G, Li S, Zu Y, Zhang W & Jia M, *J Phys Chem C*, 113 (2009) 9345.

37 Sukpanish P, Lertpanyapornchai B, Yokoi T & Ngamcharussrivichai C, *Mater Chem Phys*, 181 (2016) 422.

38 Kovalevsky A V, Populoh S, Patricio S G, Thiel P, Ferro M C, Fagg D P, Frade J R & Weidenkaff A, *J Phys Chem C*, 9 (2015) 4466.

39 Cao T, Huang P, Zhang K, Sun Z, Zhu K, Yuan L, Chen K, Chen N & Li Y, *J Mater Chem A*, 6 (2018) 3435.

40 Ma Y, Wu Z, Wang H, Wang G, Zhang Y, Hu P, Li Y, Gao D, Pu H, Wang B & Qi X, *CrystEngComm*, 21 (2019) 3982.

41 Xia Q X, Fu J, Yun J M, Mane R S & Kim K H, *RSC Adv*, 7 (2017) 11000.

42 Takahara Y, Kondo J N, Takata T, Lu D & Domen K, *Chem Mater*, 13 (2001) 1194.

43 Ahmed M A, Abou-Gamra Z M & Salem A M, *J Environ Chem Eng*, 5 (2017) 4251.